HYDROLOGICAL PROCESSES
Hydrol. Process. **27**, 1854–1865 (2013)
Published online 27 March 2013 in Wiley Online Library
(wileyonlinelibrary.com) DOI: 10.1002/hyp.9792

Modelling incoming radiation on a linear disturbance and its impact on the ground thermal regime in discontinuous permafrost

T. J. Williams* and W. L. Quinton

Centre for Cold Regions and Water Science, Wilfrid Laurier University, 75 University Ave West, Waterloo, Canada, N2L 3C5

Abstract:

Human-induced disturbances and climate-driven warming have resulted in unprecedented permafrost thaw in the zone of discontinuous permafrost. In a peatland environment south of Fort Simpson, NWT, we study the contribution of increases in incoming radiation to the ground surface, caused by removal of the tree canopy along linear disturbances, to changes in the ground thermal regime. A physically based understanding of thaw processes along linear disturbances is required in order to better understand the slow recovery of lines in this environment and to be able to efficiently reduce this impact during future resource exploration. The impact of increases in incoming radiation are examined through the development of a model (seismic incoming radiation model) to quantify these inputs, which are then used to drive the one-dimensional coupled atmospheric-surface-subsurface model COUP. Results of this study show that incoming radiation (shortwave + longwave) is increased by up to 11% in a typical cutline compared to an undisturbed canopy. Relative to potential changes in near-surface soil moisture, these increases in radiation do not appear to be an important control of permafrost thaw along linear disturbances. Field observations confirm that increased permafrost thaw on disturbances often occur irrespective of variations in incoming radiation. Copyright © 2013 John Wiley & Sons, Ltd.

KEY WORDS permafrost thaw; seismic exploration; solar radiation; forest canopy; peatlands

Received 30 September 2012; Accepted 25 February 2013

INTRODUCTION

Along the southern margins of discontinuous permafrost, resource exploration has produced linear disturbances in the form of pipelines, winter roads, and seismic cutlines which collectively form an extensive network of treeless corridors. The lack of recovery of older linear disturbances and a demand for continued exploration has raised concerns regarding the environmental impact of individual seismic lines and networks (Salmo Consulting, 2004). The rate at which seismic lines recover toward their pre-disturbance condition is in part affected by their characteristics determined at the time of disturbance, such as their orientation, width, and possible surface treatments. In recognition of this, government agencies have produced guidelines for industry on seismic practises aimed at reducing their impact (Aboriginal Affairs and Northern Development Canada (AANDC), 2011). However, the existing literature that such guidelines are based on has largely focused on the ecological impacts (James and Stuart-Smith, 2000; Dyer *et al*., 2001; Machtans, 2006) as opposed to changes in the ground thermal regime, and the energy-based studies have largely been conducted in taiga and tundra environments with shrub vegetation (Raynolds and Felix, 1989; Kemper and Macdonald, 2009; Jorgenson *et al*., 2010), or in the forested regions of the Mackenzie Delta uplands with thick and stable permafrost (Gold and Lachenbruch, 1973; Hernandez, 1973). As such, the applicability of such guidelines to the wetland-dominated southern margin of discontinuous permafrost is unknown. This is a potentially critical omission considering that this region supports the largest human population, has the highest rates of industrial development, and is undergoing the highest rates of warming (Zhang *et al*., 2000) and resulting land-cover change of anywhere in the Arctic region.

The southern permafrost boundary migrated northward by about 120 km between 1964 and 1990 (Kwong and Gan, 1994). The authors of that 1994 study conducted a detailed trend analyses which demonstrated that the disappearance of permafrost is largely the result of climate warming. Subsequent studies in the southern fringe of permafrost near Fort Simpson, Northwest Territories, Canada indicate a ~23% reduction in the extent of permafrost between 1947 and 2000 (Robinson, 2002). Elsewhere in the Fort Simpson region, at Scotty Creek, Quinton *et al*. (2011) observed a 27% reduction in the extent of permafrost plateaus within a 1 km^2 area between 1947 and 2008. Chasmer *et al*. (2011) noted that plateau retreat at Scotty occurred preferentially along edges with southeast to westerly aspects and suggested that this spatial pattern of thaw was driven by spatial variations of incoming radiation received at the ground surface. Assuming this is the case, understanding the factors influencing the spatial pattern of radiation received at the ground surface is an important first step toward reducing the environmental impact of linear disturbances, since this new understanding

*Correspondence to: T.J. Williams, Centre for Cold Regions and Water Science, Wilfrid Laurier University, 75 University Ave West, Waterloo, Canada.
E-mail: tjw2@alumni.sfu.ca

could be applied to the design of future disturbances so that their impact can be minimized.

For cutlines, the canopy is removed to a width that is dependent on the size of machinery used to clear the line and drill the shot holes. Conventional techniques for seismic exploration typically created lines that were 6–10 m wide; however, low-impact techniques using 'enviro-drills' require lines between 2 and 3 m wide, and heli-portable drill rigs require only minimal foot access along large stretches of the line (AECOM, 2009). Such low-impact techniques increase the cost of exploration, and while in Canada they have been applied frequently over the past decade in Alberta and northern British Columbia, they have been less common in the Territories.

Numerous studies have examined the effects of a forest canopy on incoming shortwave (SW) (0.2–3.5 μm) and longwave (LW) (3.5–100 μm) radiation for the purpose of predicting snowmelt. These have included a wide range of northern coniferous species under low sun angles and provide a solid theoretical foundation, as well as methods to calculate incoming radiation values on linear disturbances. Forest canopies reduce SW irradiance to the surface by reflection and absorption, while generally increasing LW irradiance through emission of absorbed energy (Pomeroy *et al*., 2009). Essentially, the canopy acts as a filter and transformer of radiation, absorbing a portion of incoming SW radiation and re-emitting it in all directions in the LW form. The emissivity of canopy material always remains close to 1; therefore, the LW emission is based on the temperature of the canopy.

Canopy heating is mainly confined to trunk and branch woody material, while foliage remains near air temperature (Ellis, 2011). Tree temperatures may be important for incoming radiation to canopy gaps, because the edges of these gaps can be exposed to large fluxes of SW radiation. A study of a forest clearing in the southern Canadian Rocky Mountains observed differences of approximately 10% in LW radiation on opposite sides of a clearing due to preferential warming of the south facing canopy edge (Ellis, 2011).

The total incoming radiation arriving at the ground surface of a gap in the tree canopy is effected by the relationship between the size of the gap and the sun angle (Lawler and Link, 2011). At high sun angles, even a small gap may receive incoming SW fluxes similar to an open area, while receiving increases in LW radiation from the surrounding heated canopy, such that there becomes greater all-wave radiation in the gap than in an open area. At low sun angles, gaps may become well shaded while still being in a fairly open area, and thus receive less radiation than at the ground surface below a continuous canopy.

Studies aimed at better understanding ground thaw along linear disturbances have primarily avoided calculations of incoming radiation. A study by Smith and Riseborough (2010) modelled the ground thermal regime at several points along the Norman Wells pipeline, approximately 25 km east of the Scotty Creek study site referred to above, using the two-dimensional Temp-W model. The model output compared well with the observation of 3 m of vertical thaw over the 25 years since the pipeline was installed and the model predicted continued permafrost degradation assuming on-going climate warming scenarios. However, the pipeline in question is a 25 m wide disturbance that primarily has radiation inputs equal to that of an open area. Smith and Riseborough were able to drive the model without considering incoming radiation. Instead, they established a relationship between surface temperature and air temperature for an off-disturbance site and applied a 2 °C increase in surface temperature for the disturbance, which they based on field measurements.

Results of ground thaw modelling in this region have demonstrated a sensitivity of peat soils to changes in soil moisture conditions, where wetter conditions increased the ground thaw rate (Burgess and Smith, 2000; Woo *et al*., 2006). The simulations by Woo *et al*. (2006) for permafrost-affected peatlands in the Fort Simpson region indicated that moving the water table from a depth of 20 cm to the ground surface would produce a 40 cm increase in active layer depth. Active layer thaw monitoring at Scotty Creek by Wright *et al*. (2009) also indicated that seasonal thaw was greater in wet areas of a peat plateau than in drier areas and found that the average end of season thaw depth was greater in wet than in dry years.

The overall goal of this study is to quantify the variation of incoming radiation along linear disturbances and compare its impact on the ground thermal regime with variations in soil moisture using site validated models. This will be achieved by the following specific objectives: (1) measure incoming radiation (SW and LW) in a treeless bog and on undisturbed (i.e. tree-covered) plateaus to observe natural radiation regimes at these two end-members; (2) develop a simple model to simulate the incoming SW and LW irradiance for any point on a linear disturbance and validate the model with field measurements of the same; (3) apply the validated seismic incoming radiation model (SIRM) to compute the radiation input to the ground surface of linear disturbances of different size, orientation, and surrounding canopy characteristics to gain a greater understanding of the site factors that control incoming radiation; and (4) use the computed radiation input to drive the one-dimensional coupled atmospheric-surface-subsurface model COUP (Jansson and Karlberg, 2001), and use the latter to compare the impact of disturbance-induced changes to soil moisture and radiation regimes on ground thaw.

STUDY SITE

The study site is located 50 km south of Fort Simpson, NWT, in the headwaters of Scotty Creek (61°18`N, 121°18`W) (Figure 1). The mean annual temperature at Fort Simpson (class 'A' station Meteorological Service of Canada) is −3.2 °C (1960–2010) with a mean annual total precipitation of 372 mm, of which 45% falls as snow. As is typical of the southern margin of permafrost in Canada, Scotty Creek is a peatland environment where permafrost exists only beneath plateaus that rise 1–2 m above the surrounding wetlands and thus maintains an unsaturated layer near the ground surface which thermally insulates the permafrost below. Plateaus support a thin black spruce

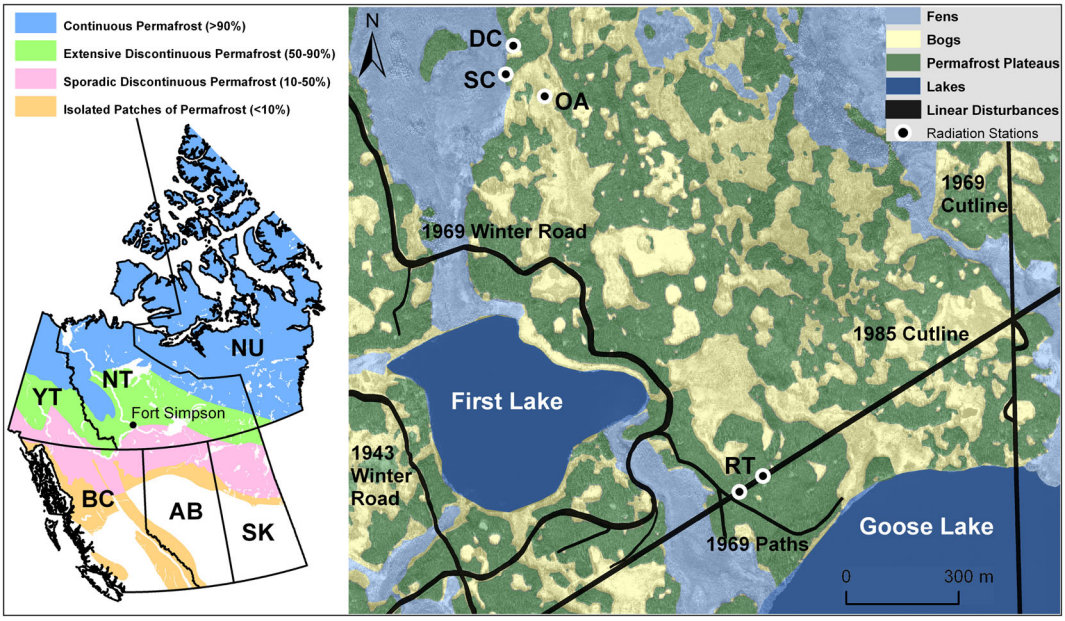

Figure 1. Location of the study site 50 km south of Fort Simpson, Northwest Territories in the Lower Liard Valley (permafrost classification obtained from Geologic Survey of Canada, 2002). Map on the right shows the Scotty Creek study area with land classifications overlaying WorldView2 satellite imagery. Radiation stations are located beneath a dense canopy (DC), sparse canopy, and in an open area (OA), and two roving radiation transects (RT) are located on the 1985 cutline

canopy (*Picea mariana*), a shrub layer (mostly *Ledum groenlandicum*), and a surface cover of lichens and mosses. The sparse tree canopy typically has an average height of 3–5 m and average sky view factor of 0.75–0.87 (Chasmer *et al.*, 2011). As the margins of these plateaus thaw, the ground surface subsides into the surrounding wetlands causing the tree canopy to become waterlogged and die and preserving the relationship between the location of permafrost and the location of the black spruce canopy.

Fens and bogs are permafrost free land cover types that receive drainage from the surrounding plateaus and typically contain water tables at or near the ground surface. Bogs can vary greatly in size from small isolated bogs that are surrounded by a single plateau, to large bogs that border multiple plateaus and connect with fens. Bogs are covered in mosses (mostly *Sphagnum fuscum* and *Pleurozium schreberi*) and primarily act to store water in a nutrient poor environment. Fens are broad channels 50 to >100 m wide that are dominated by sedge vegetation, often with a floating peat mat, and act as the drainage network to move water slowly towards the basin outlet.

The distinctive hydrologic functions of the three land cover types at Scotty Creek result from their differences in the presence of permafrost, which is relatively impermeable in this environment. Therefore, the loss of permafrost along linear disturbances is likely to alter the storage and movement of water. This potential to alter the basin hydrology is high given that the density of winter roads and seismic cutlines at Scotty Creek is 0.875 km/km^2, more than five times the natural drainage density of the basin (Quinton *et al.*, 2011).

METHODS

Field instrumentation

An open area (i.e. treeless) meteorological station located in a bog measures and records wind speed (Met One 014A), air temperature, and relative humidity (Vaisala RH and temperature probe HMP45C212) all at 2 m above the surface. The bog station, along with two plateau stations within relatively dense and sparse canopies, records incoming and outgoing radiation (Kipp and Zonen CNR1) to an accuracy of ±10% of daily totals. All three towers are attached to CR10X Campbell Scientific loggers which average data over 30 s intervals and output the data every half hour. Precipitation is measured on a plateau within a canopy gap (Geonor T-200B Precipitation Gauge) at half hour intervals. Data is summarized over a thaw season that is defined to begin upon the snow free condition and continue until the end of August.

Measurements of incoming radiation on cutlines were made between March 29 and June 22, 2011 using a roving radiation station equipped to measure incoming LW radiation (Kipp & Zonen CGR3 Pyrgeometer) and incoming SW radiation (Kipp & Zonen CMA6 Albedometer). The radiometers were attached to a Campbell Scientific CR1000 datalogger with a half-hour output of averaged data. The station was deployed on eight different points on the 1985 cutline and three points in adjacent forested areas (Figure 1), remaining at each site for a minimum of 3 days. Each point is related to the above canopy condition represented by the bog tower; the roving radiation instruments were placed next to the bog station for three days to confirm accuracy between these instruments. Differential GPS measurements were used to

locate the position for each of the roving radiation sites to a horizontal accuracy of ±10 cm. Additionally, permafrost table depth on August 31st (2 m graduated steel rod) and depth-integrated soil moisture from 0 to 5 cm (site calibrated Delta-T Theta-Probe ML2x) was measured along these same transects.

The height of the surrounding canopy for each site was derived from a 1 m horizontal resolution LiDAR-based canopy height model. The width and orientation of the disturbances were measured directly in the field for each of the roving sites. The canopy view factor was measured directly from digital hemispherical photographs (Cannon fisheye lens), analyzed to six rings (CanEye software) to measure the fraction of canopy cover.

Instantaneous tree temperature measurements along the edges of linear disturbances and ground surface temperatures were made using an Apogee Infrared Radiometer (IRR-P), which has a manufacturer's accuracy of ±0.2 °C. Tree temperatures were recorded of black spruce barks facing towards the disturbance at breast height, with averages calculated for each side of the disturbance from ten trees sampled. The procedure was repeated 22 times between March 29 and May 24, 2011 on two disturbances: the 1985 cutline with a primarily east–west orientation and the 1969 winter road where there is a north–south orientation (Figure 1).

Modelling incoming radiation

The proportion of above canopy irradiance that reaches the ground surface referred to as the canopy transmittance is often defined using the sky-view factor, V_f (Reifsnyder and Lull, 1965), which is the proportion of hemispherical sky that an observer on the ground would see for any given location ($V_f = 1$ for a completely open area, $V_f = 0$ for a canopy that blocks the entire sky). Previous studies have determined the sky-view factor from direct measurement using hemispherical photographs (Essery *et al.*, 2008), remotely sensed data (Essery *et al.*, 2008), and also by empirical equations relating V_f to the leaf area index (Sicart *et al.*, 2004).

When modeling incoming radiation beneath a canopy gap, the direct and diffuse components of SW radiation must be considered separately (Essery *et al.*, 2008). Diffuse beam radiation can be reasonably expressed using the sky-view factor because diffuse radiation is assumed to reach the surface equally from all directions; however, the extinction of the direct SW beam is dependent on the position of the sun at any given time relative to the width and height of the gap, such that the proportion of energy reaching the surface varies considerably with time. For canopy gaps, this direct beam extinction has been expressed as a function of the path length that the beam travels through the canopy, calculated geometrically from the position of the sun and size of the canopy gap (Ellis, 2011; Lawler and Link, 2011). This approach assumes random orientation of canopy material, such that the direct beam extinction is dependent only on the path length and a density coefficient.Incoming SW and LW radiation is calculated for any point on a linear disturbance using the seismic incoming radiation model (SIRM). Building on the approach of Lawler and Link (2011) and Ellis (2011), the direct SW beam into a canopy gap is calculated as,

$$K_b = K_{b0}\tau(\theta) = K_{b0}\ e^{-L'\ \gamma} \tag{1}$$

where θ is the solar elevation (0–90°), L′ is the optical depth of the forest, K_{bo} is the above canopy direct SW component, and γ is the path length correction factor (where $\gamma \geq 0$). When $\gamma < 0$, the direct beam travels through the opening in the canopy gap, Equation (1) does not apply, and $\tau(\theta) = 1$. The optical depth (L′) is a density constant for the canopy, such that it is equal to the negative logarithm of the transmissivity (τ) when the distance traveled through the canopy is equal to the height of the canopy. Assuming that the sky-view factor is equal to the transmissivity, L′ is calculated for each roving measurement site from digital hemispherical photographs.

The path length correction factor (γ) in Equation (1) represents the proportion of distance that the direct beam must travel through the canopy relative to the height of the canopy (Figure 2). Adjusting the calculation of γ for a linear disturbance,

$$\gamma = \frac{1}{\sin\theta} - \frac{x_1'}{h\cos\theta} \tag{2}$$

where x_1' is the distance to the disturbance edge in the direction of the direct solar beam (Figure 2) so that,

$$x_1' = \frac{x_1}{\cos(\lambda)} \tag{3}$$

where x_1 is the distance to the disturbance edge, and λ (0–90°) is the difference between the solar azimuth (β) and the line perpendicular to the orientation of the linear disturbance. Combining Equations (2) and (3),

$$\gamma = \frac{1}{\sin\theta} - \frac{x_1}{h\cos\theta\cos\lambda} \tag{4}$$

The incoming SW diffuse (K_d) and LW (L_{IN}) radiation are expressed in terms of the sky-view factor (V_f), which for a circular canopy gap with a homogenous canopy where the transmissivity is constant in all directions, can be calculated using the expression of Reifsnyder and Lull (1965),

$$V_f = 2\int_0^{\pi/2} \tau(\theta)\ \ \cos\theta\sin\theta\ \ d\theta \tag{5}$$

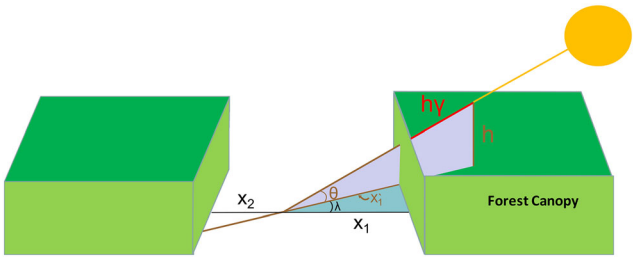

Figure 2. Sketch of a linear disturbance between surrounding forest canopies identifying the variables used to calculate the path length correction factor (γ), where h is the height of the canopy, $x_{1,2}$ are the distances to the canopy edges, θ is the solar elevation, and λ is the solar azimuth relative to the orientation of the disturbance

For a non-circular canopy gap, such as a linear disturbance, the sky-view factor must be calculated by integrating over the entire hemisphere, 0–90° solar elevation (θ) and 0–360° solar azimuth (β), such that

$$V_f = \frac{1}{\pi}\int_0^{\pi/2}\int_0^{2\pi} \tau(\theta,\beta)\cos\theta\sin\theta \; d\beta \; d\theta \qquad (6)$$

with the assumption that the sky-view factor is equal to the transmissivity of the canopy, and that τ can be defined using the exponential from Equation (1). Using this definition of τ, the integral in Equation (6) does not have a closed-form solution, so SIRM approximates a solution using 1 degree intervals of θ and β. V_f can be calculated for any point on a linear disturbance given the position on the disturbance and the height and density of the surrounding canopy.

The sky-view factor remains constant over time for a given location, allowing the diffuse SW radiation to be calculated as,

$$K_d = K_{d0} \; V_f \qquad (7)$$

where K_{d0} is the above canopy diffuse radiation. Similarly, the incoming LW radiation is calculated using the Stefan–Boltzman Law,

$$L_{IN} = \; V_f L_0 + \left(1 - V_f\right)\varepsilon_c \sigma {T_c}^4 \qquad (8)$$

where L_0 is the above canopy LW irradiance, ε_c is the effective canopy emissivity, T_c is the canopy temperature, and σ is the Stefan–Boltzman constant. The canopy emissivity is referred to as 'effective' in order to acknowledge that Equation (7) neglects the small reflective LW component; therefore, $\varepsilon_c = 0.98$, which is slightly larger than the actual emissivity (Pomeroy *et al.*, 2009).

SIRM is run at 30 min intervals with sun positions calculated using well established solar equations (National Oceanic and Atmospheric Administration (NOAA), 2012) that considers latitude, longitude, date, and time to compute the solar azimuth and elevation (θ). The above canopy incoming SW (K_0) and LW radiation (L_0) used to run the model will be represented by measurements taken from the open area (bog) station beginning at start of the 2010 thaw season. The proportion of direct and diffuse SW radiation required for Equations (1) and (6) is calculated using the BRL model, an empirically derived universal model (Ridley *et al.*, 2010) such that,

$$K_{do} = K_o\left(1 + e^{(-5.38+6.63k_t+0.006AST-0.007\theta+1.75K_t+1.31\Psi)}\right)^{-1} \qquad (9)$$

where k_t is the half hourly atmospheric transmissivity, AST is the apparent solar time, θ is the solar elevation, K_t is the daily atmospheric transmissivity, and ψ is the average of atmospheric transmissivity of the previous and following time steps.

In addition to the calculation of incoming radiation for a single point on a linear disturbance using SIRM, the radiation is also expressed as an average across the entire width of the disturbance. This is done by separating the cross section into ten equally sized segments, simulating the midpoint of each segment using SIRM, and calculating an average across all ten points.

Modelling the ground thermal regime

We modelled the ground thermal regime using COUP, a coupled one-dimensional mass and energy model based on well-known physically based equations (Jansson and Karlberg, 2001). The model divides the soil into layers, assumes the conservation of mass and energy, and allows flow to occur as a result of gradients in water potential (Darcy's Law) or temperature (Fourier's Law). All properties of the snow and soil are parameterized, and the model is driven from meteorological observations. The bog station is used to provide air temperature, relative humidity, and wind speed, and the radiation inputs are given as the outputs of the calculations discussed in the previous section.

In order to best account for the effects of soil moisture on surface temperature, we allow the surface temperature to be calculated as an iterative solution of the surface energy balance, such that,

$$Q^* = R_n + Q_A = Q_G + Q_H + Q_E \qquad (10)$$

where R_n is the net radiation, Q_A is the advection energy from rainfall, and $Q_{G,H,E}$ are the ground, sensible, and latent heat fluxes. Snow albedo is determined in COUP depending on the snow surface age and air temperature, while snow-free albedo is determined using a site calibrated equation where the albedo varies from 0.13 to 0.19 depending on the surface soil moisture. The individual energy components are calculated using the following equations,

$$Q_G = \frac{2k_h(T_s - T_1)}{\Delta z_1} \qquad (11)$$

$$Q_H = \rho_a C_p \frac{(T_s - T_a)}{r_{as}} \qquad (12)$$

$$Q_E = \frac{\rho_a C_p}{\gamma_c}\frac{\left(e_{surf} - e_a\right)}{r_{as}} \qquad (13)$$

where k_h is the thermal conductivity, T_s is the surface temperature, T_1 is the temperature of the upper most soil layer, Δz_1 is the thickness of the uppermost soil layer, ρ_a is the density of air, C_p is the heat capacity of air, T_a is the air temperature, r_{as} is the aerodynamic resistance, γ_c is the psychometric constant, e_{surf} is the vapour pressure of the surface, and e_a is the actual vapour pressure of the air (Jansson and Karlberg, 2001).

Validation of the model was performed using data from the Sparse Canopy Station where incoming LW and SW radiation is measured (Kipp and Zonen CNR1) and initial

temperatures are given as observed values at depths of 5, 10, 15, 20, 25, 30, 40, 50, 60, and 70 cm (Campbell 107B thermistors). The modeled drainage is set to best replicate soil moisture conditions at the Sparse Canopy Station observed at depths of 10 and 20 cm (Hydro-Probe II), which were wet relative to most plateau locations, with an average volumetric soil moisture of 55% at 10 cm and 73% at 20 cm (averaged from snow-free condition to the end of August). Outputs of the validation run are compared to measured outgoing radiation, ground heat flux (Campbell HFT3) and frost table progression as interpreted using the ground thermistors. The HFT3 was site calibrated as described in Hayashi *et al*. (2007). Validation was limited to the summer thaw period due to equipment failure of the HFT3 during the winter.

All COUP model runs used thermal (Hayashi *et al*., 2007) and hydrological (Quinton *et al*., 2008) soil properties based on studies conducted on Scotty Creek peat plateaus. The model begins prior to snowmelt on March 3, 2010 and is allowed to run for one full year from the time where the surface becomes snow free. The scenario we are interested in representing is the period immediately following the creation of the disturbance, where we assume that all vegetation has been removed and that the initial subsurface temperatures are equal to those observed on an undisturbed peat plateau. Our COUP simulations do not consider any ground surface vegetation effects on water or energy exchange.

RESULTS

Radiation measurements

Cumulative total radiation (MJ/m^2) from meteorological stations representing three canopy conditions (open area, sparse, dense) are summarized in Table I from 2008 to 2010. On an annual basis, incoming LW as a percentage of the total incoming radiation accounts for 69% at the treeless bog, 76% below the sparse canopy, and 82% below the dense canopy. These values are lowest during the thawing period, but even then LW still accounts for 60% of the open area radiation.

The incoming radiation beneath the sparse and dense canopies remained a consistent proportion of the open area radiation between the two observed measurement years. The surface beneath the sparse canopy received a greater proportion of open area (i.e. above canopy) SW radiation (73%) than the ground surface beneath the dense canopy (52%). However, these differences are partially offset by the increased incoming LW radiation beneath the denser canopy. Overall, the ground below the sparse canopy received about 95% of the all-wave above canopy radiation, while at the ground below the dense canopy, 90% of the above canopy value was received. These values were lowest during the thaw season when the fraction of above canopy all-wave was 93% and 88% respectively beneath the sparse and dense canopies.

Tree temperatures

Figure 3 illustrates a strong relationship between air temperature and tree trunk temperature at breast height along the edges of linear disturbances. Tree trunk temperatures remained approximately 5 °C warmer than the air over the range of observed air temperatures (−10 to 18 °C). There were cases where the tree trunk temperature became much more than just ~5 °C above the air temperature. These outliers occurred when the edge of a disturbance with old growth trees was aligned perpendicular to direct sun beam. When the disturbance edge is in the shade, the difference between air temperature and trunk temperature remains small (~5 °C). Since the effective emitting temperature of the canopy is less than the skin temperature of the tree barks (Ellis, 2011), and the time period where substantial warming occurs appears to be short, we assume that canopy temperature is equal to air temperature for the purpose of modelling incoming LW radiation.

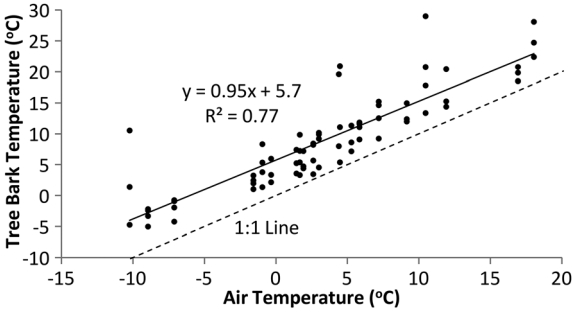

Figure 3. Relationship between tree trunk temperature and air temperature from instantaneous measurements of black spruce trees along the edges of linear disturbances, where each point represents an average of ten trees. The solid line represents the best fit, and the dashed line is the 1:1 line. Using standardize major axis regression, tree bark temperatures are shown to be significantly greater than air temperatures ($P < 0.0001$)

Table I. Radiation components (MJ/m^2) expressed as a fraction of open area (above canopy) radiation, for a relatively sparse and dense canopy from 2008 to 2010

		K_{IN}	L_{IN}	$K_{IN} + L_{IN}$	Albedo (α)	L_{OUT}	Rn
2008/09	Open area	3752	8362	12 113	0.33	9373	1496
Sparse canopy	2743 *(0.73)*	8718 *(1.04)*	11 461 *(0.95)*	0.23	9513	1322 *(0.88)*	
Dense canopy	1898 *(0.51)*	9030 *(1.08)*	10 928 *(0.90)*	0.27	9509	899 *(0.60)*	
2009/10	Open Area	3658	8563	12 221	0.28	9643	1554
Sparse canopy	2652 *(0.73)*	8905 *(1.04)*	11 557 *(0.95)*	0.19	9751	1292 *(0.83)*	
Dense canopy	1955 *(0.53)*	9185 *(1.07)*	11 141 *(0.91)*	0.23	9734	961 *(0.62)*	

Incoming radiation along linear disturbances

Figure 4 shows incoming radiation measurements and SIRM simulations of the same, at points along two radiation transects across the 1985 cutline (Figure 1). All results are displayed as a fraction of the treeless bog station (i.e. above canopy) radiation. Observed SW radiation on cutlines was greatest (0.83–0.94) in the centre and south-facing side of the east–west oriented cutline, while variation in observed LW radiation was minimal among all sites. LW radiation increased slightly (<5%) towards the edges of the cutline, but no difference was observed between LW radiation on a south or north facing side. This is consistent with the results of tree trunk temperatures, which suggests that daytime warming of the canopy edges is generally small (~5 °C).

The accuracy of SIRM across the cutline improved towards the centre of the line where the results become less dependent on the position of the measurement relative to nearby trees. Overall, 7 of the 11 roving points were modelled within 5% of the observed values for SW radiation, and all of the points were modelled within 3% of the observed LW radiation. Additionally, all of the points were modelled within 5% for the all-wave (i.e. SW + LW) incoming measured values, because the majority of the sites where SW was underestimated also overestimated LW and vice-versa.

The greatest uncertainty for simulating incoming radiation to these disturbances comes from defining the density of the canopy. The density of the canopy at Scotty Creek is difficult to quantify with considerable variation across a plateau due to the clumping of trees. Attempts to measure canopy density with LiDAR data did not compare well to digital hemispherical photographs, because the thin trees are often undetected by the LiDAR signal (Chasmer *et al.*, 2008). This limited the area where we were able to validate SIRM to sites where hemispherical photographs had been taken.

Applying SIRM over a single thaw season (May 15th–August 31st), the total incoming radiation across the entire width of a cutline is expressed in terms of an average flux (Figure 5), which shows that the factor that most controls the total radiation inputs is the line width to tree height ratio. The all-wave incoming radiation increases rapidly over narrow disturbances, such that the average flux for a width to height ratio of 1 is about 8% greater than an undisturbed canopy. At a width to height ratio of 2, the average incoming radiation approaches that of an open area, and so further increases in the ratio have little effect on the average incoming radiation for the disturbance.

The typical width to height ratio at Scotty Creek is around 1.5–2 for seismic lines, and 2–2.5 for winter roads. This model suggests that these disturbances receive relatively large inputs of radiation, at around 95–98% of the above canopy values. By reducing the width of these disturbances by 50%, the model calculates that the average incoming radiation could be reduced by between 2 and 4%, depending on the density of the surrounding canopy, which becomes more important with lower width to height ratios. The denser canopies effectively reduce the SW radiation component without a corresponding increase in LW radiation. However, in wider disturbances, the incoming radiation contains a greater proportion of direct SW radiation, reducing the importance of canopy density. For width to height ratios > 2, the canopy density has a minimal effect on the average all-wave radiation reaching the ground surface (Figure 5).

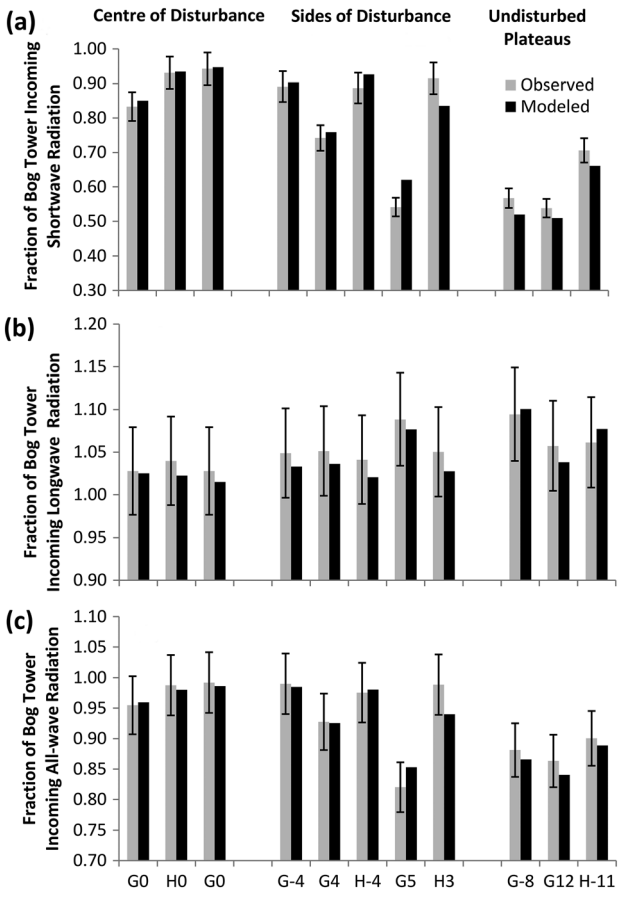

Figure 4. Modelled (black bars) and measured (grey bars) incoming (a) shortwave, (b) longwave, and (c) all-wave radiation for two cross sections (G and H) on the 10 m wide 1985 cutline (Figure 1), where the site number represents the distance (in metres) from the centre of the cutline (+ towards south). The y-axis represents the fraction of incoming energy relative to the treeless bog station (above canopy) during the observed time period. The error bars represent a 5% deviation in energy from the observed values

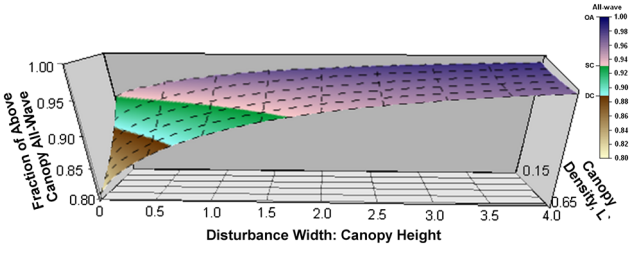

Figure 5. Modelled (SIRM) incoming all-wave radiation, expressed as an average over the entire width of a north–south disturbance during the thaw season for various width to canopy height ratios (x-axis), and canopy densities (z-axis). The y-axis displays the radiation as a fraction of the above canopy input into the model. Colour boundaries represent the fraction of incoming radiation observed beneath the sparse canopy (SC), dense canopy (DC), and bog open area (OA) meteorological stations as shown in the legends

Without considering warming of the surrounding tree canopy in SIRM, there is no mechanism for the average LW radiation to vary with orientation. For very narrow disturbances (w:h ≤ 0.5), SIRM also shows no differences in modelled SW radiation between the two orientations. However, for typical disturbances (w:h >0.5), more direct SW radiation reaches an east–west oriented line compared to a north–south line, resulting in a ~1% difference in all-wave radiation between the two disturbances.

Despite not having a large effect on the total radiation inputs to a disturbance, the orientation plays an important role in the distribution of radiation along a cross section of a disturbance, as well as the magnitude of peak radiative flux (Figure 6). The magnitude of the modelled peak all-wave radiation is 2–3% greater for an east–west orientation, reaching upwards of 99% of the above canopy values on a 10 m wide disturbance. Additionally, the north–south lines have a nearly symmetrical distribution of all-wave radiation, with the peak occurring in the middle of the line; whereas, the east–west line varies considerably between the two sides and peaks towards the south-facing edge. The increases in all-wave radiation on the east–west line extends several metres into the forest on the south-facing side, allowing portions of the off-disturbance surface to get more incoming radiation than is received on the shaded side of the disturbance.

COUP validation

Figure 7 compares COUP simulations to field observations at the Sparse Canopy Station, beginning at the end of snowmelt and continuing until the end of August. The observed cumulative net radiation during this period (1056 MJ/m^2) was slightly greater than the cumulative simulated value (1012 MJ/m^2), due primarily to a greater loss of LW radiation modelled in late July and August.

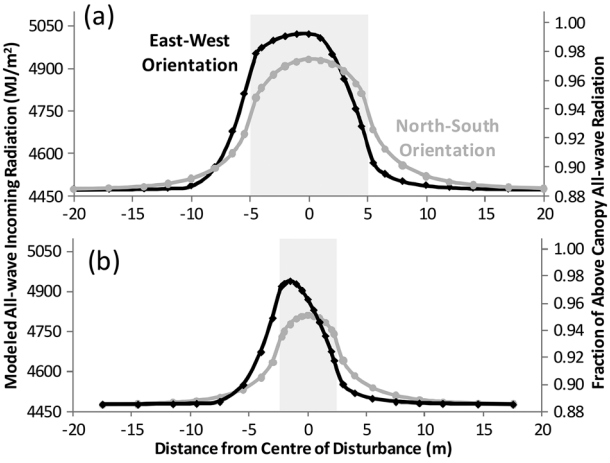

Figure 6. Modelled (SIRM) thaw season incoming all-wave radiation across hypothetical disturbances that are (a) 10 m wide, and (b) 5 m wide; each with a canopy height of 5 m, and a canopy density, L` = 0.3. The black line represents an east–west orientation, the grey line a north–south orientation, and the shaded background indicates the extent of the disturbance

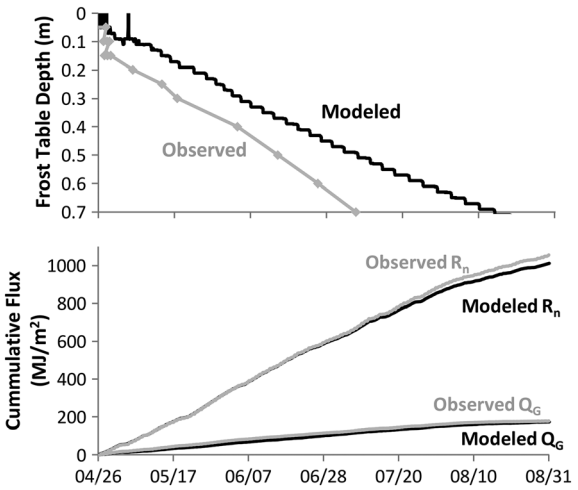

Figure 7. Comparing COUP model simulations to observed data at the sparse canopy station for the 2010 thaw season for (a) frost table progression inferred from the progression of the zero-degree isotherm and (b) cumulative ground heat flux and ground surface net energy balance. The figure does not show the progression of the frost table beyond 0.70 m, because this is the deepest thermister in the field

Additionally, the cumulative ground heat flux compared well between the observed heat flux plate (178 MJ/m^2) and the model (174 MJ/m^2) throughout the summer.

The greatest difference between the COUP simulations and the observed data occurred with the progression of the frost table, where the simulated active layer underestimated the observed rate (Figure 7). This is particularly the case early on in the season with the active layer between 0 and 0.15 m, and again later in the season below 0.40 m depth. Given the similarity in observed and modeled Q_g, this suggests that the ice content in the field may not be as high as what was set in COUP for the initial conditions. It is possible that this section of plateau contains a perennially unfrozen zone beneath the active layer, which could have been a consequence of ground disturbance during the installation of the sensors. Additionally, there may be other sources of thaw energy unrepresented in the model such as lateral heat advection or thermal conduction through tree root networks; however, neither of these possible additional energy sources should be as important for simulating ground thaw on a freshly cleared disturbance. It appears that the discrepancy between the COUP model and observations beneath the sparse canopy are a result of a failure to define initial conditions and should not affect the results that focus on differences in the ground heat flux.

COUP results

Table II shows the results of COUP model simulations using four different incoming radiation scenarios for both dry and wet soil conditions. The water table for the wet soil condition remained near the ground surface throughout the summer, while for the dry condition, it averaged 24 cm below the ground surface with an average saturated thickness of 8 cm. Three of the radiation scenarios are outputs of SIRM discussed in

Table II. COUP model results using four different radiation scenarios and two moisture conditions. All energy values are cumulative seasonal fluxes (MJ/m^2); ground, latent, and sensible fluxes are also expressed as a fraction of the net energy balance. Mean water table and surface temperatures are calculated from April 26th– August 31st, the mean air temperature during this period was 14.1 °C

Simulation #	1	2	3	4	5	6	7	8
Radiation scenario	Middle of 10 m wide disturbance (SIRM)		Middle of 5 m wide disturbance (SIRM)		Middle of 2 m wide disturbance (SIRM)		No disturbance, observed dense canopy	
Incoming all-wave, MJ/m^2 (fraction of above canopy)	5837 (0.99)		5651 (0.96)		5428 (0.92)		5203 (0.88)	
Soil moisture	Dry	Wet	Dry	Wet	Dry	Wet	Dry	Wet
Mean water table depth (m)	−0.25	−0.02	−0.25	−0.02	−0.24	−0.01	−0.24	−0.01
Max. frost table depth (m)	0.63	0.91	0.61	0.89	0.59	0.89	0.57	0.87
Mean surface temp. (°C)	17.6	15.3	16.9	14.7	16.1	14.3	15.4	13.3
Snow-free date	Apr 26	Apr 26	Apr 27	Apr 27	Apr 28	Apr 28	Apr 29	Apr 29
Surface energy balance in MJ/m^2 from April 26th to August 31st (fraction of Q*)								
Net radiation, Rn	922	1164	824	1048	708	894	590	784
Ground heat flux, Qg	123 (.13)	178 (.15)	121 (.14)	176 (.16)	118 (.16)	177 (.19)	116 (.19)	172 (.21)
Latent heat flux, Qe	290 (.31)	798 (.67)	281 (.33)	744 (.70)	269 (.37)	636 (.70)	237 (.39)	619 (.77)
Sensible heat Flux, Qh	524 (.56)	209 (.18)	436 (.52)	145 (.14)	335 (.46)	94 (.10)	250 (.41)	1 (.001)

previous sections using 5 m canopy heights, L` = 0.3, and east–west orientations for: (1) the middle of a 10 m wide disturbance (fraction of above canopy all-wave radiation = 0.99); (2) the middle of a 5 m wide disturbance (0.96); and (3) the middle of a 2 m wide disturbance (0.92). The fourth radiation scenario represents an undisturbed canopy and used measured, rather than modelled, values of incoming radiation from the dense canopy station (0.88).

The net radiation varies considerably between the different COUP simulations depending on the soil moisture and amount of incoming radiation (Table II). Comparing the two extreme incoming radiation scenarios (dense canopy, 10 m disturbance), there was an 11% difference in incoming radiation input data during the thaw season, which magnified to percentage differences in net radiation (R_n) of 39% (wet condition) and 44% (dry condition). However, the wetness of the soil also had a large impact on R_n, with an average difference of 25% between the dry and wet conditions.

The lower values of R_n for dry conditions are a result of more outgoing LW radiation resulting from higher ground surface temperatures. The dry soils have a lower heat capacity and less demand for energy from evaporation, causing the surface to heat up and give off more sensible heat and LW radiation. The average surface temperature in the simulations was 1.5 – 2.5 °C warmer for the dry condition than the wet.

The moisture condition also has a strong influence on the magnitude of ground heat flux, with an average difference of 38% between dry and wet conditions, due to the increased thermal conductivity of wet organic soils. The effect of soil wetness variations on the ground heat flux appears to far out-weigh the influence of variation of incoming radiation. For the wet condition, the ground heat flux is within 2 MJ/m^2 among the three modelled disturbances. Radiation becomes slightly more important for the dry conditions where Q_G increases by about 1 MJ/m^2 per 70 MJ/m^2 increase in incoming radiation. However, there remain small changes relative to the differences in Q_G between the wet and dry conditions. The end of season frost table depth for the dry condition increased by 6 cm (±2 cm thickness of computational soil layers) from the dense canopy to the middle of a 10 m disturbance, yet for any single radiation input, changing the soil moisture to the wet condition increased the frost table by 28–30 cm for a single season.

The partitioning of energy in the COUP simulations showed considerable variation during the thaw season due to the availability of water and the position of the frost table. Early in the thaw season, while the water supply is high and the capacity of the active layer to store additional input is low due to its largely frozen and saturated state (Hayashi *et al.*, 2007), latent fluxes dominate the energy balance. In July and August, the modelled soils that are allowed to drain become dry, allowing them to heat up and release a greater amount of energy as sensible heat.

The ground surface temperature and ground heat flux in COUP are dependent on the wind speed. The previous simulations were obtained using wind inputs from an open area (bog station) that averaged 1.7 m/s throughout the modelled period. When wind speeds from a small opening on a plateau were used to run the model (average 0.8 m/s), evaporation is decreased, causing the ground surface temperature to rise, which decreased the net radiation and increased the ground heat flux. For the lower wind speeds under wet conditions, Q_G increased by an average of 3.2 MJ/m^2 (7%), and for dry conditions, Q_G increased by an average of 3.5 MJ/m^2 (11%). The actual wind speed on disturbances is likely somewhere in between these two cases, dependent on the size and orientation of the disturbance. If there are considerable differences in wind speed between different disturbances, this may represent a substantial source of variation between the ground heat flux on disturbances, which could be equal to or greater in importance to the variation in incoming radiation.

When modelled over an entire year, the ground heat flux continues to be more dependent on the soil moisture regime than the incoming radiation (Figure 8). Dry model simulations resulted in an annual ground heat flux between 9 and 15 MJ/m^2, while wet simulations ranged from 44 to 56 MJ/m^2. Differences in radiation are small during the winter and have very little effect on the ground thermal regime; however, snow depth is widely known to be an important component of the winter ground thermal regime. Driven by measurements of precipitation, the COUP model simulated a peak winter snow depth of 120 cm, which appears to be an overestimation of the snowpack. It is also an above average year for snowfall in Fort Simpson, which may explain why all our model runs show an annual positive ground heat flux even for the dry simulations. With a thinner snowpack, there would be increased winter freezing and a reduced annual Q_G.

The steep negative slope of the cumulative Q_G simulations in October and November (Figure 8) represents a period of strongly negative ground heat flux where there was minimal snow cover. In mid-October, there was a seven day period where 47 mm of precipitation was measured with air temperatures close to 0 °C. The results presented in Figure 8 produced a snow depth of 20 cm by the end of this event, similar to what was reported for Fort Simpson (Meteorological Service of Canada (MSC), 2012). However, by slightly adjusting the parameters in the model that determines precipitation phase, and causing the mid-October precipitation to become a predominately snow event, the annual Q_G for each of the eight simulations increases by >40 MJ/m^2. This represents a potentially significant source of yearly variation for the ground thermal regime and supports the fact that the extent of winter freezing is strongly dependent on the timing and amount of fall snow accumulation.

Permafrost thaw

Field observations of permafrost thaw support the ground thermal modelling results that incoming radiation alone is not sufficient to cause substantial thaw. Figure 9 compares the all-wave radiation modelled by SIRM to observations of soil moisture and depth to permafrost as measured at the end of August. Despite the increased incoming radiation on the south-facing side of the disturbance, permafrost thaw is greater on the north-facing side of the disturbance. Coarse woody debris piled on the south-facing edge of the disturbance allowed this portion of the line to remain dry and maintain permafrost within 1 m of the ground surface.

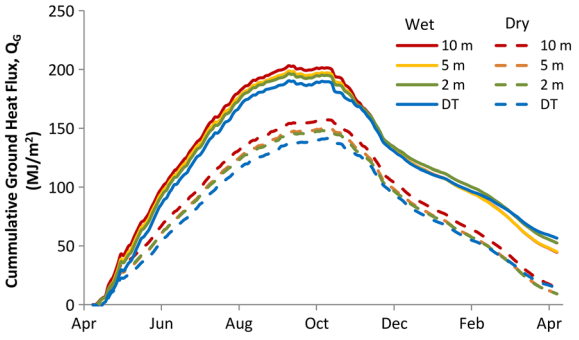

Figure 8. Modeled ground heat flux in COUP over a 1 year period (Apr 10, 2010 – Apr 9, 2011) for the wet (solid lines) and dry (dashed lines) conditions and four different radiation inputs representing SIRM simulations for the middle of a 10 m, 5 m, and 2 m disturbance, as well as observed inputs from the dense canopy station

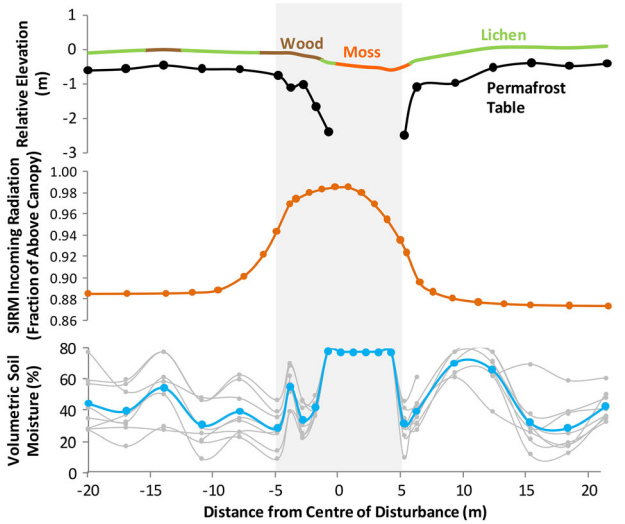

Figure 9. Modelled all-wave thaw season incoming radiation (SIRM) across the 10 m wide 1985 cutline (RT in Figure 1), compared with measurements of the ground surface elevation, permafrost table depth (August 31st), and soil moisture (upper 5 cm). Individual measurements of soil moisture (8 between May 8 and 22) are shown in grey, with the average in blue. The shaded background indicates the extent of the disturbance (treeless condition). Wood indicates course woody debris is the dominant cover on the ground surface

Similar relationships were observed on an east–west oriented 1985 cutline south of Goose Lake. At this site, both edges of the cutline were covered in woody and maintained frozen ground near the surface. On July 25th, thaw was measured to be slightly greater on the shaded side of the disturbance (average 70 cm, n = 15) than on the south-facing side (average 53 cm, n = 15). Only on the middle of the disturbance was thaw observed to extend beyond 2 m beneath the ground surface.

These sites are typical of cutlines at Scotty Creek since unlike the edges of plateaus, the edges of cutlines have not begun to thaw laterally. This is evident from piles of coarse woody debris and tree tags that mark the width of the original cutlines. Only on the older and highly degraded abandoned winter roads is there evidence from leaning trees that lateral thaw is beginning to occur.

DISCUSSION

The COUP simulations suggest that increases in soil moisture were the likely cause of initial permafrost thaw along linear disturbances at Scotty Creek. The increases in incoming all-wave radiation calculated for these disturbances resulted in small increases in the ground heat flux, which may be at least partially offset by faster wind speeds that increases turbulent transfer and decreases Q_G. The importance of soil moisture

implies that in order to best maintain permafrost on these disturbances, focus should be directed towards minimizing the surface impact during construction and avoiding changes to drainage patterns.

Focusing on the initial thaw period of a freshly cut linear disturbance meant, we could apply initial moisture and temperature conditions from observed plateau sites and allowed us to avoid any talik development. The COUP simulations of the present study, as well as field observations by Wright (2009), have shown that the ground heat flux is strongly dependent on the presence of a frozen active layer near the ground surface. When the zero-degree isotherm is well below the ground surface (i.e. after active layer thaw when there is a perennially unfrozen zone beneath), the temperature gradient close to the ground surface is reduced, along with the ground heat flux. This process will act as a negative feedback to permafrost thaw. As long as the soil moisture remains the same, a deeper permafrost table should result in a reduced rate of permafrost thaw. Thus, it would not be appropriate to take the modelled rates of thaw from our single year of simulations and apply them to subsequent years.

Another factor that may influence the ground thermal regime over time is the regrowth of vegetation. The COUP simulation assumed bare soils; however, the presence of moss, lichen, shrubs, and eventually small trees would each have different controls on the ground surface temperature, soil moisture, and turbulent heat exchanges. Additionally, coarse woody debris or wood mulch on the disturbance may alter the surface properties and remains an area where further research is required.

Due to the age of the disturbances at our site, it is difficult to know what ground surface properties followed removal of the tree canopy. COUP simulations used soil properties that were measured for an undisturbed plateau; however, it is likely that soil compaction would have occurred and resulted in decreased porosity, reduced infiltration, and wetter soils. The extent to which the water table would have adjusted after disturbance is unknown, and the two moisture conditions used in this model are hypothetical, but given the observation that repeated walking over the surface is sufficient to compact the peat so that it remains saturated, this indicates that these soils are highly sensitive to compaction.

Without studying how these disturbances respond beyond the initial period following disturbance, we cannot rule out the cumulative impact of increasing radiation on permafrost thaw; however, we can speak to the relative importance of radiation as compared to soil moisture. The iterative solution of surface temperature in COUP calculated a 2 °C difference in surface temperature between radiation for the dense tower and the middle of a 10 m disturbance, which is the same as the temperature differences observed along the Norman Wells Pipeline south of Fort Simpson (Smith and Riseborough, 2010). Having confidence in our ground surface temperature results, we can say that increases in soil moisture following disturbance in this environment have far greater potential to induce permafrost thaw than changes in incoming radiation. In order to reduce the environmental impact of future linear disturbances, further research is required to study the causes of initial increases in soil moisture along these disturbances. Questions remain as to what effect removal of the canopy itself has in increasing soil moisture through reductions in evaporation (Vitt *et al*., 1999) compared to moisture increases from surface compaction.

The relative importance of soil moisture compared to incoming radiation may also be applicable towards understanding permafrost thaw that is occurring along the edges of plateaus at Scotty Creek. It does not appear likely that any input of radiation would be sufficient to contribute substantially to the rate of thaw that is occurring along these edges of plateaus, which have been observed to thaw laterally at rates up to 1.3 m/year with 10 m thick permafrost (Quinton *et al*., 2011).

Our hypothesis is that disturbances that have had more vertical permafrost thaw are more likely to become hydrologically connected with the surrounding wetlands and receive inputs of relatively warm water. The lateral influx of energy associated with this process may explain why older disturbances appear to be thawing into the surrounding undisturbed canopy and younger (or less degraded) disturbances maintain their original width. Similarly with the edges of permafrost plateaus, we suspect that lateral energy transfer of flowing water in bogs and channel fens is a primary contributor to the pattern of thaw observed at Scotty Creek.

CONCLUSIONS

1. Plateaus receive less SW and more LW incoming radiation than adjacent areas without a canopy due to the absorption and emission of energy by the canopy. Observations of all-wave incoming radiation over two thaw seasons measured these differences to be a 7% reduction at the Sparse Canopy Station and an 11% reduction at the Dense Canopy Station.
2. We developed an incoming radiation model for linear disturbances which compared well with field data over short time periods. Given the size and position of a disturbance and the surrounding canopy characteristics, this model is able to calculate inputs for any point on or near a linear disturbance.
3. Canopy height and disturbance width are the greatest controls on all-wave incoming radiation to a linear disturbance. The orientation of the disturbance affects the distribution of radiation across the line, with the potential to cause high inputs on a south-facing side, but does not substantially affect the total inputs to the disturbance. Typical cutlines and winter roads at Scotty Creek ($\geq$10 m wide) can receive peak all-wave radiation inputs equal to around 99% of above canopy values.
4. Due to the limited range of incoming radiation caused by the thin canopy at Scotty Creek, incoming radiation does not appear to play a large role in increasing ground thaw following a disturbance. The two factors which predominantly control the ground thermal regime are soil moisture and winter snowfall. During the summer thaw season, increases in soil moisture for these organic soils have a much greater potential to increase ground thaw compared to increases in radiation, due to the strong

relationship between soil moisture and thermal conductivity. Maintaining dry soils at the ground surface of plateaus is necessary in order to maintain permafrost in this environment.

ACKNOWLEDGEMENTS

We wish to acknowledge the financial support of the Canadian Foundation for Climate and Atmospheric Sciences and the Natural Sciences and Engineering Research Council. We also acknowledge the logistical support provided by the National Water Research Institute (Saskatoon) and by Gerry Wright and Roger Pilling of the Water Survey of Canada (Fort Simpson). The Aurora Research Institute is gratefully acknowledged for their assistance in obtaining a research license. We also wish to thank the Denedeh Resources Committee, Deh Cho First Nation, Fort Simpson Métis Local #52, Liidlii Kue First Nation, and the Village of Fort Simpson for their support of this project. In particular, we thank Allan Bouvier and Allen Bonnetrouge of the Liidli Kue First Nation, and Chief Stanley Sanguez of the Jean-Marie River First Nation for their continued support. We thank Dr. Laura Chasmer, Dr. Chris Hopkinson, and the Applied Geomatics Research Group for their assistance. Julian Kanigan of Aboriginal and Northern Development Canada, Dr. Jennifer Baltzer, and Dr. Aaron Berg are also thanked for their insightful comments.

REFERENCES

Aboriginal Affairs and Northern Development Canada (AANDC). 2011. Northern land use guidelines: Northwest Territories seismic operations, volume 09a, Government of the Northwest Territories: Yellowknife; 48.

AECOM. 2009. Considerations in developing oil and gas industry best practices in the north. Government of Canada: Whitehorse; 36.

Burgess MM, Smith SL. 2000. Shallow ground temperatures. In The physical environment of the Mackenzie Valley, Northwest Territories: a base line for the assessment of environmental change, Dyke LD, Brooks GR (eds). Geological Survey of Canada: Ottawa; 69–103.

Chasmer L, Quinton W, Hopkinson C, Petrone R, Whittington P. 2011. Vegetation canopy and radiation controls on permafrost plateau evolution within the discontinuous permafrost zone, Northwest Territories, Canada. *Permafrost and Periglacial Processes* **22**: 199–213. DOI: 10.1002/ppp.724

Salmo Consulting. 2004. Deh Cho cumulative effects study, Phase 1: Management indicators and thresholds. Deh Cho Land Use Planning Committee: Calgary; 152.

Dyer SJ, O'Neill JP, Wasel SM, Boutin S. 2001. Avoidance of industrial development by woodland caribou. *Journal of Wildlife Management* **65**: 531–542. DOI: 10.2307/3803106

Ellis C 2011. Radiation and snowmelt dynamics in mountain forests. PhD Thesis, University of Saskatchewan; 214.

Essery R, Pomeroy J, Ellis C, Link T. 2008. Modelling longwave radiation to snow beneath forest canopies using hemispherical photography or linear regression. *Hydrological Processes* **22**: 2788–2800. DOI: 10.1002/hyp.6930

Essery R, Rutter N, Marks D, Link T, Pomeroy J, Melloh R, Rowlands A, Bunting P, Hardy J. 2008. Radiative transfer modeling of a coniferous canopy characterized by airborne remote sensing. *Journal of Hydrometeorology* **9**: 228–241. DOI: 10.1175/2007JHM870.1

Geological Survey of Canada (GSC). 2002. Permafrost thickness in Canada. retrieved on May 25, 2012 from: www.geogratis.cgdi.gc.ca.

Gold LW, Lachenbruch AH. 1973. Thermal conditions in permafrost- A review of North American literature. In *North American contribution permafrost second international conference*. National Academy of Sciences: Washington; 23–25.

Hayashi M, Quinton WL, Wright N, Goeller N. 2007. A simple heat-conduction method for simulating the frost-table depth in hydrological models. *Hydrological Processes* **21**: 2610–2622. DOI: 10.1002/hyp.6792

Hernandez H 1973. Natural plant recolonization of surficial disturbances, Tuktoyaktuk Peninsula Region, Northwest Territories. *Canadian Journal of Botany* **51**: 2177–2196. DOI: 10.1139/b73-280

James ARC, Stuart-Smith AK 2000. Distribution of caribou and wolves in relation to linear corridors. *Journal of Wildlife Management* **64**: 154–159. DOI: 10.2307/3802985

Jansson RE, Karlberg L. 2001. Coupled heat and mass transfer model for soil-plant-atmosphere systems. Royal Institute of Technology, Dept. of civil and environmental engineering: Stockholm; 445.

Jorgenson J, Hoef J, Jorgenson M. 2010. Long-term recovery patterns of arctic tundra after winter seismic exploration. *Ecological Applications* **20**: 205–221. DOI: 10.1890/08-1856.1

Kemper JT, Macdonald SE. 2009. Directional change in upland tundra plant communities 20–30 years after seismic exploration in the Canadian low-arctic. *Journal of Vegetation Science* **20**: 557–567. DOI: 10.1111/j.1654-1103.2009.01069.x

Kwong YTJ, Gan TY. 1994. Northward migration of permafrost along the Mackenzie highway and climate warming. *Climate Change* **26**: 399–419. DOI: 10.1007/BF01094404

Lawler R, Link T. 2011. Quantification of incoming all-wave radiation in discontinuous forest canopies with application to snowmelt prediction. *Hydrological Processes* **25**: 3322–3331. DOI: 10.1002/hyp.8150

Machtans CS. 2006. Songbird Response to Seismic Lines in the western boreal forest: a manipulative experiment. *Canadian Journal of Zoology* **84**: 1421–1430. DOI: 10.1139/Z06-134

Meteorological Service of Canada (MSC) 2012. National climate data archive of Canada, Environment Canada: Dorval, Quebec.

National Oceanic and Atmospheric Administration (NOAA). 2012. Solar position calculator, retrieved from: www.srrb.noaa.gov/highlights/sunrise/calcdetails.html.

Pomeroy JW, Ellis C, Marks D, Link T, Granger R, Rowlands A, Hardy J. 2009. The impact of coniferous forest temperature on incoming longwave radiation to melting snow. *Hydrological Processes* **23**: 2513–2525. DOI: 10.1002/hyp.7325

Quinton WL, Hayashi M, Carey SK. 2008. Peat hydraulic conductivity in cold regions and its relation to pore size and geometry. *Hydrological Processes* **22**: 2829–2837. DOI: 10.1002/hyp.7027

Quinton WL, Hayashi M, Chasmer LE. 2011. Permafrost-thaw-induced land-cover change in the Canadian subarctic: implications for water resources. *Hydrological Processes* **25**: 152–158. DOI: 10.1002/hyp.7894

Raynolds MK, Felix NA. 1989. Airphoto analysis of winter seismic disturbance in Northeastern Alaska. *Arctic* **42**: 362–367. DOI: 10.2307/40510858

Reifsynder WE, Lull HW. 1965. Radiant energy in relation to forests. US Dept. of Agriculture technical bulletin No. 1344, US government printing office: Washington; 111.

Ridley B, Boland J, Lauret P. 2010. Modeling of diffuse solar fraction with multiple predictors. *Renewable Energy* **35**: 478–483. DOI:10.1016/j.renene.2009.07.018

Robinson SD. 2002. Peatlands of the Mackenzie Valley: permafrost, fire, and carbon accumulation. In *Long-term dynamics and contemporary carbon budget of northern peatlands*. Yu ZC, Bhatti JS, Apps MJ (technical coordinators). Natural Resources Canada, Canadian Forest Service Report NOR-X-383: Edmonton; 21–24.

Sicart JE, Marks D, Link T, Pomeroy JW, Hardy J, Essery RLH. 2004. A sensitivity study of daytime net radiation during snowmelt to forest canopy and atmospheric conditions. *Journal of Hydrometeorology* **5**: 774–784. DOI:10.1007/s-011-0213-x

Smith SL, Riseborough DW. 2010. Modelling the thermal response of permafrost terrain to right-of-way disturbance and climate warming. *Cold Regions Science and Technology* **60**: 92–103. DOI:10.1016/j.coldregions.2009.08.009

Vitt DH, Halsey LA, Zoltai SC. 1999. The changing landscape of Canada's western boreal forest: the current dynamics of permafrost. *Canadian Journal of Forest Research* **30**: 283–287. DOI: 10.1139/x99-214

Woo M-K, Mollinga M, Smith S. 2006. Simulating active layer thaw in a boreal environment. *Géographie physique et Quaternaire* **60**: 9–17. DOI:10.7202/016361ar

Wright N. 2009. Water and energy fluxes from a permafrost peat plateau: examining the controls on runoff generation. PhD Thesis, Simon Fraser University; 158.

Zhang X, Vincent LA, Hogg WD, Niitsoo A. 2000. Temperature and precipitation trends in Canada during the 20th century. *Atmosphere-Ocean* **38**: 395–429. DOI: 10.1080/07055900.2000.9649654

